Haacke, E. M., Brown, R. W., Thompson, M. R., and Venkatesan, R. 1999. *Magnetic resonance imaging, physical principles and sequence design*. New York: John Wiley & Sons.
Liang, Z.-P., Boada, F. E., Constable, R. T., Haacke, E. M., Lauterbur, P. C., and Smith, M. R. 1992. Constrained reconstruction methods in MR imaging. *Rev. Magn. Reson. Med.* 4: 67–185.
McGibney, G., Smith, M. R., Nichols, S. T., and Crawley, A. 1993. Quantitative evaluation of several partial Fourier reconstruction algorithms used in MRI. *Magn. Reson. Med.* 30: 51–59.
Noll, D. C., Nishimura, G. D., and Macovski, A. 1991. Homodyne detection in magnetic resonance imaging. *IEEE Trans. Med. Imaging* 10: 154–163.

### RELATED SECTIONS

Section 8.1 Frequency-Encoding Gradients
Section 8.2 Phase-Encoding Gradients
Section 13.1 Fourier Reconstruction

## 13.5 Phase Difference Reconstruction

MRI, unlike CT, is a phase-sensitive imaging modality. After the Fourier reconstruction of the MR raw data, each pixel in the complex image has both a magnitude and a phase. The phase of the MR image is discarded when the standard magnitude reconstruction is performed. There can be, however, very useful information encoded into the phase. For example, the phase map can yield information about $B_0$ homogeneity, which is used for shimming, or about fluid flow, as described in Section 15.2 on phase contrast angiography. Emerging applications such as MR temperature mapping (Ishihara et al. 1995) and MR elastography (Muthupillai et al. 1995) also use the phase information.

In day-to-day MR acquisitions there are invariably unwanted contributions to the image phase, which can arise from system imperfections such as gradient eddy currents (Section 10.3) or from unavoidable physical effects such as chemical shift, magnetic susceptibility variations, and the concomitant (i.e., Maxwell) field (Section 10.1). These unwanted contributions make a phase map more difficult to interpret because the desired information is often overwhelmed by the unwanted phase. Acquiring two independent data sets and then forming a *phase difference* map can address this problem. As the name implies, the phase difference map is obtained by displaying the difference between a pair of phase images on a pixel-by-pixel basis (Moran et al. 1985). The goal is to accentuate the desired phase while canceling the unwanted phase. For example, to produce a $B_0$ map for shimming, two gradient-echo data sets are acquired with identical parameters, except that the TE is varied. The phases of the two complex images are subtracted to yield the phase difference map (Figure 13.33). Similarly, for phase-contrast angiography, the flow-encoding gradient (Section 9.2) is modified between the two acquisitions and a phase difference map is reconstructed, as described in Section 15.2.



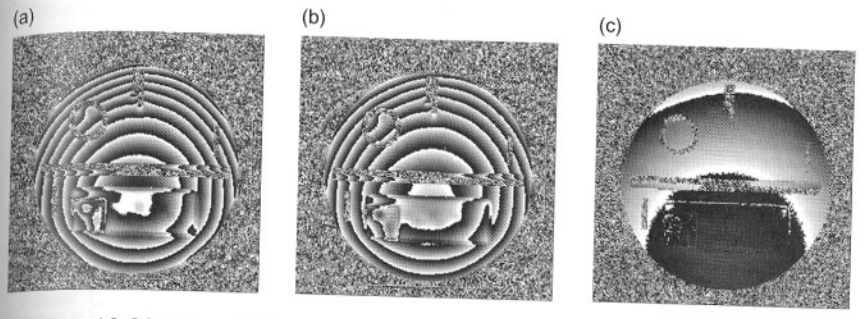


FIGURE 13.33 Phase difference reconstruction. The phase images (a) and (b) are subtracted on pixel-by-pixel basis to yield the phase difference map (c). The phase difference operation can cancel unwanted phase errors while accentuating useful phase information (e.g., about $B_0$ or flow). Note how the outline of the phantom is more easily discernable on (c). In practice, the intermediate step of reconstructing the individual phase images (a) and (b) is generally not necessary, and an algorithm such as Eq. (13.113) is used instead.

### 13.5.1 QUANTITATIVE DESCRIPTION

The heart of any phase difference reconstruction is the per-pixel arctangent operation that yields the phase map. The tangent function is periodic and has discontinuities at $(n + 1/2)\pi$, $(n = 0, \pm 1, \pm 2, \ldots)$, so the output of arctangent function is defined over a limited range, for example, $-\pi/2 < \arctan(x) < \pi/2$. (The range of the phase is increased to $[-\pi, \pi]$ when a four-quadrant arctangent function is used, as described later in this section.) In any case, the values of the phase outside the primary range are represented by a value in the primary range, or *alias*. Aliasing in the phase map is accompanied by discontinuities called *phase wraps*, which are abrupt transitions, for example, between $\pi$ and $-\pi$ when the four-quadrant arctangent is used. For computational efficiency, and to minimize the number of phase wraps, an optimal phase difference reconstruction should employ only a single arctangent operation per pixel. Also, because of the discontinuities, it is desirable to perform operations such as the phased-array multiple coil combination and the concomitant-field phase correction *prior* to calculating that arctangent. The steps involved in a phase difference reconstruction, described next, are summarized in Figure 13.34.

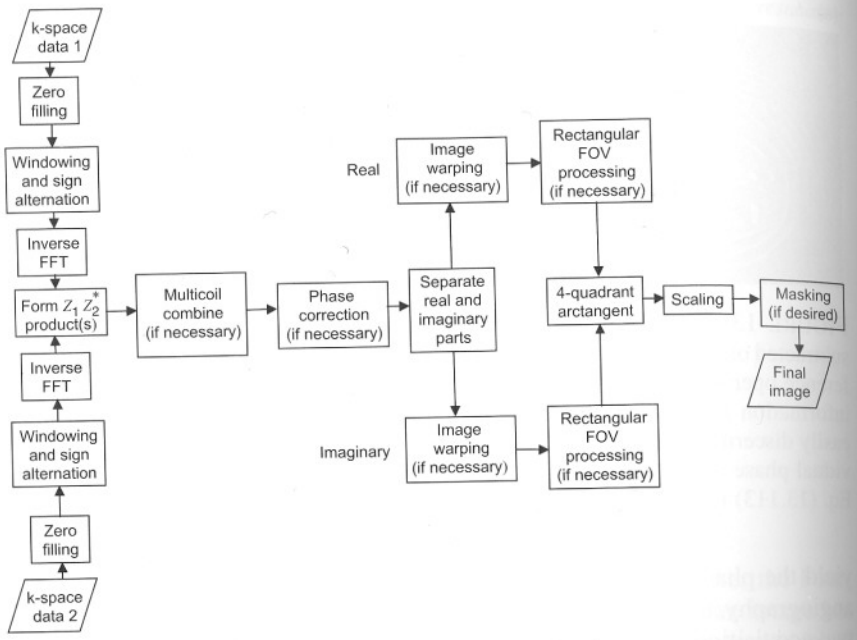


FIGURE 13.34 Flowchart for phase difference reconstruction steps.

*Arctangent Operation* Suppose two k-space raw data sets are acquired, and we want to form a phase difference map from them. The data sets are first sign alternated and zero-filled, as described in Section 13.1, and then separately Fourier transformed to yield two independent complex images. We consider a particular pixel and denote its complex value in the first image by:

$$Z_1 = x_1 + iy_1 = \rho_1 e^{i\phi_1} \tag{13.109}$$

and in the second image by:

$$Z_2 = x_2 + iy_2 = \rho_2 e^{i\phi_2} \tag{13.110}$$

The phase difference for this pixel can be calculated by:

$$\Delta\phi = \arctan\left(\frac{y_1}{x_1}\right) - \arctan\left(\frac{y_2}{x_2}\right) = \phi_1 - \phi_2 \tag{13.111}$$

but Eq. (13.111) uses two arctangent operations per pixel, which is computationally costly and can introduce extra phase wraps. Instead, it is preferable to



form a complex ratio and then extract the phase:

$$\Delta\phi = \measuredangle\left(\frac{Z_1}{Z_2}\right) \equiv \arg\left(\frac{Z_1}{Z_2}\right) = \measuredangle(\rho_1\rho_2 e^{i(\phi_1-\phi_2)}) = \arctan\left(\frac{\mathrm{Im}\,(Z_1/Z_2)}{\mathrm{Re}\,(Z_1/Z_2)}\right) \tag{13.112}$$

Because the complex conjugate and the inverse of the complex number $Z_2$ both have the same phase (i.e., $-\phi_2$), Eq. (13.112) can be recast into a somewhat simpler form:

$$\Delta\phi = \measuredangle(Z_1 Z_2^*) \equiv \arg(Z_1 Z_2^*) = \arctan\left(\frac{\mathrm{Im}\,(Z_1 Z_2^*)}{\mathrm{Re}\,(Z_1 Z_2^*)}\right) \tag{13.113}$$

Substituting Eqs. (13.109) and (13.110) into Eq. (13.113) yields an expression for the phase difference in terms of the real and imaginary components of the two complex values (O'Donnell 1985):

$$\Delta\phi = \arctan\left(\frac{x_2 y_1 - x_1 y_2}{x_1 x_2 + y_1 y_2}\right) \tag{13.114}$$

Whenever Eq. (13.113) or (13.114) is evaluated on a digital computer or array processor, it is useful to use the four-quadrant arctangent function, which is generically known as ATAN2 in several programming languages, including *C* (Kernighan and Ritchie 1998). The four-quadrant arctangent function takes two input arguments: the numerator and the denominator of the arctangent function. For example, Eq. (13.113) can be rewritten as:

$$\Delta\phi = \arctan\left(\frac{\mathrm{Im}(Z_1 Z_2^*)}{\mathrm{Re}(Z_1 Z_2^*)}\right) = \mathrm{ATAN2}\left[\mathrm{Im}\left(Z_1 Z_2^*\right), \mathrm{Re}\left(Z_1 Z_2^*\right)\right] \tag{13.115}$$

The four-quadrant arctangent function tests the signs of its two individual arguments before forming their ratio. For example, if the numerator and denominator are both positive, then ATAN2 returns a value in first quadrant, but, if they are both negative, then it returns a value in third quadrant. In this way, the dynamic range is extended from $(-\pi/2, \pi/2)$ to $[-\pi, \pi]$, that is, to all four quadrants in the complex plane. Any phase difference value that lies outside the range $[-\pi, \pi]$ will be aliased back into the primary range by adding or subtracting multiples of $2\pi$. For example, if the true phase difference value is $3.5\pi$, then $-0.5\pi = 3.5\pi - 4\pi$ will be displayed. (Aliasing in phase-contrast angiography is discussed in more detail in Section 15.2.) Note that use

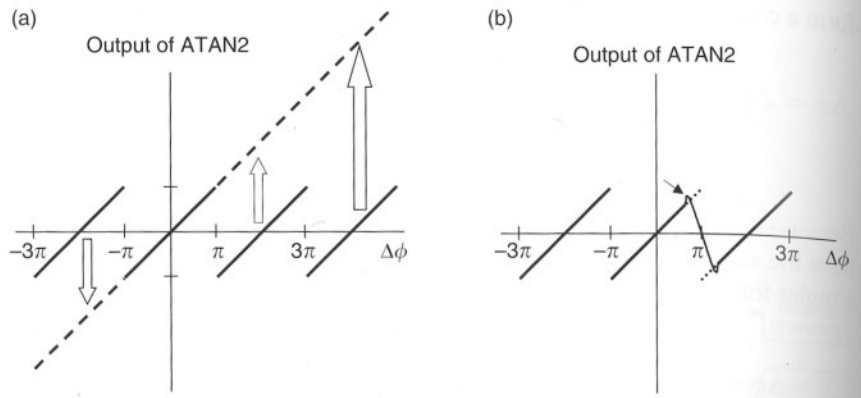


FIGURE 13.35 A plot of the output of the four-quadrant arctangent function versus the true phase difference. (a) When the true phase difference is in $[-\pi, \pi]$, the two are equal. When the true phase difference lies outside $[-\pi, \pi]$, the two differ by an integer multiple of $2\pi$. This is phase aliasing, and the sharp transitions are phase wraps. Phase aliasing can be unwrapped by adding or subtracting the proper multiple of $2\pi$ (hollow arrows), so the output of the arctangent function and the true phase difference are equal over a longer stretch (dashed line). (b) A pitfall of interpolating phase images. If the phase image is interpolated (e.g., for image warping or for minification for rectangular field of view), overshoot (arrow) can occur at the aliasing boundary. Then the interpolated phase image can never be properly unwrapped. Instead, it is preferable to interpolate the real and imaginary images prior to the arctangent operation.

of the ATAN2 function compared to the conventional arctangent function can reduce the occurrence of phase wraps simply because of its increased range.

The process of restoring the phase difference values in the range $[-\pi, \pi]$ back to their true values is called *phase unwrapping* and is illustrated in Figure 13.35a. A detailed description of the postprocessing step of phase unwrapping is beyond the scope of this section, but several effective algorithms have been described for medical images (e.g., see Liang 1996 and Section 17.3).

Another advantage of the ATAN2 function is that instead of reporting a divide-by-zero error when the second argument is zero, it returns the correct value of $\pm\pi/2$, depending on the sign of the first argument. (It is always advisable to check the specific documentation for the ATAN2 function that is being used because some details can vary among implementations.)

*Phased-Array Multiple Coil Data* Many acquisitions use multiple coils arranged in a phased array. The optimal acquisition and processing of these data requires multiple receivers, which produce multiple channels of MR data.



An algorithm to reconstruct a phase difference map from this multichannel data is described here.

Adopting the notation of Section 13.1, we denote the receiver channels by the index $j$ and define $\sigma_j^2$ to be the measured noise variance for the $j$th channel, as explained in Section 13.1. Then the phase difference map can be calculated (Bernstein et al. 1994) from the expression:

$$\Delta\phi = \measuredangle\left(\sum_j \frac{Z_{1j}Z_{2j}^*}{\sigma_j^2}\right) = \text{ATAN2}\left(\text{Im}\sum_j \frac{Z_{1j}Z_{2j}^*}{\sigma_j^2}, \text{Re}\sum_j \frac{Z_{1j}Z_{2j}^*}{\sigma_j^2}\right) \tag{13.116}$$

Note that any spatially dependent phase contribution from an individual coil receive $B_1$ field is cancelled in Eq. (13.116) when the phase difference is formed.

Performing the multiple-coil combination prior to the arctangent operation, as in Eq. (13.116), has an advantage that is illustrated in the following example. Suppose the true phase difference $\Delta\phi$ is near the aliasing boundary of $\pi$ (or 180°) and there are two receiver channels. Suppose further that because of noise, the individual phase differences that would be extracted from the two receivers straddle the aliasing boundary:

$$\begin{aligned}\Delta\phi_1 &= \pi - \varepsilon \\ \Delta\phi_2 &= -\pi + \varepsilon\end{aligned} \tag{13.117}$$

where $\varepsilon \ll 1$. Simply averaging the phases gives the incorrect result, because the sum:

$$\Delta\phi = \Delta\phi_1 + \Delta\phi_2 = \pi - \varepsilon + (-\pi + \varepsilon) = 0 \tag{13.118}$$

If, however the multiple-receiver combination is made before the arctangent operation according to Eq. (13.116), a better estimate to the correct value of $\Delta\phi = \pi$ is obtained. From Eq. (13.116), the phase difference for this two-receiver case can be written:

$$\Delta\phi = \measuredangle\left(\sum_{j=1}^{2} \frac{\rho_{1j}\rho_{2j}e^{i\Delta\phi_j}}{\sigma_j^2}\right) \tag{13.119}$$

Assuming that the noise variances and image magnitudes have only weak dependence on the index $j$, it is a good approximation to remove the $\rho$s and $\sigma$s from the sum, and substituting Eq. (13.117) into Eq. (13.119) yields:

$$\begin{aligned}\Delta\phi &\approx \measuredangle(e^{i(\pi-\varepsilon)} + e^{i(-\pi+\varepsilon)}) = \measuredangle(e^{i\pi}(e^{-i\varepsilon} + e^{-2\pi i}e^{i\varepsilon})) \\ &= \measuredangle(e^{i\pi}\,2\cos\varepsilon) = \pi\end{aligned} \tag{13.120}$$

(Depending on the implementation of the ATAN2 function, the value $-\pi$ may be obtained instead. The two are equivalent because $+\pi$ and $-\pi$ differ by $2\pi$.) Since Eq. (13.120) is the correct result, this example illustrates the general rule that as many of the other operations as possible should precede the arctangent operation in a phase difference reconstruction. Another example of an operation in which this rule applies is described next.

*Correction of Predictable Phase Errors and the Concomitant Field* Even after forming the phase difference image, unwanted phase errors often remain. A common example is the phase contamination due to gradient eddy currents (Section 10.3) that can plague phase-contrast angiography. Because eddy currents are dependent on the design and calibration of the MR hardware, it is usually difficult to predict the exact spatial dependence of the phase error that is produced. Therefore, this type of phase error is often corrected by empirical fitting on the final phase difference image. For example, the constant and linear phases could be determined with a polynomial fit (Bernstein et al. 1998) of the phase difference image in a region that should have zero phase difference, such as stationary tissue in a phase-contrast angiogram. Because presumably the fitted phase is due entirely to system imperfections such as eddy currents, it is then removed with postprocessing.

Other phase errors, however, such as those produced by the concomitant (i.e., Maxwell) field, can be predicted with great accuracy because they are fundamental physics effects (Section 10.1). In that case, it is advantageous to correct for these phase errors *before* calculating the arctangent. This procedure avoids phase wraps in the phase difference map, thereby reducing the need for later phase unwrapping. Also, because the concomitant field has nonlinear spatial dependence, removing its phase error at this stage makes it easier to fit the eddy-current phase errors later. If the calculated concomitant phase error at the pixel of interest is $\phi_e$, then the phase-corrected version of Eq. (13.113) is:

$$\Delta\phi_{\text{corr}} = \angle(Z_1 Z_2^* e^{-i\phi_e}) = \text{ATAN2}\left[\text{Im}\left(Z_1 Z_2^* e^{-i\phi_e}\right), \text{Re}\left(Z_1 Z_2^* e^{-i\phi_e}\right)\right] \tag{13.121}$$

Because the phase error from the concomitant field is independent of the receiver channel number, the phase correction for the multiple coil case becomes:

$$\Delta\phi_{\text{corr}} = \angle\left(e^{-i\phi_e} \sum_j \frac{Z_{1j} Z_{2j}^*}{\sigma_j^2}\right) \tag{13.122}$$

The details of this phase correction method can be found in Bernstein et al. (1998).



*Image Warping* The image warping operation described in Section 13.1 that corrects for gradient nonlinearity can also be applied to phase difference images. As with the multiple-coil combination, it is preferable to apply the image warping prior to the arctangent operation. This is because image warping is a conformal mapping that uses an interpolation method such as cubic splines. If the image warping is applied after the arctangent operation, a phase wrap may be encountered and its sharp discontinuity can cause unwanted ringing in the image. Moreover, a phase difference image processed in this way cannot be properly unwrapped at a later time because the sharp transition between $-\pi$ and $\pi$ has been distorted (Figure 13.35b).

Suppose the warping operation on an image $I$ is denoted by the function $W(I)$. Then one strategy is to apply the warping operation separately to the real and imaginary components of the image. Thus Eq. (13.115) is modified:

$$\begin{aligned}\Delta\phi_{\text{warped}} &= \arctan\left(\frac{W\left(\text{Im}\left(Z_1 Z_2^*\right)\right)}{W\left(\text{Re}\left(Z_1 Z_2^*\right)\right)}\right) \\ &= \text{ATAN2}\left[W\left(\text{Im}\left(Z_1 Z_2^*\right)\right), W\left(\text{Re}\left(Z_1 Z_2^*\right)\right)\right]\end{aligned} \tag{13.123}$$

where $W$ should be understood to act on the entire image, rather than a single pixel. Other variations on Eq. (13.123) have also been proposed (Bernstein and Frigo 1995). Another advantage of applying the image warp separately to the real and imaginary images before the arctangent operation, as in Eq. (13.123), is that any change in image intensity caused by the warping algorithm will not affect the phase difference map.

As mentioned in Section 13.1, including the minification step in the image warp is a convenient way to reconstruct rectangular FOV images. This is true for rectangular FOV phase difference images as well.

*Image Scaling* The output of the ATAN2 function is a real, floating point (or double-precision floating point) number in the range from $-\pi$ to $\pi$. Often it is desirable to scale this output to a more convenient range by multiplying it by some constant. For example, in phase-contrast angiography, the output can be scaled so that the pixel values represent velocity in convenient units such as millimeters per second. Similarly for a $B_0$ map, we might want the pixel intensity to represent frequency offset $\delta f$ in hertz, tenths of hertz, or a convenient fraction of parts per million.

***Example 13.2*** Suppose a $B_0$ map is obtained by forming the phase difference from two gradient-echo images with values of TE equal to 10 ms and 25 ms. How should the result of the phase difference map be scaled so that each intensity count represents a frequency offset of 0.1 Hz?

***Answer*** To convert from radians to tenths of hertz, the phase difference map must be scaled according to:

$$\delta f \left[\frac{\text{Hz}}{10}\right] = \frac{10\,\Delta\phi}{2\pi\,\Delta\text{TE}} = \frac{10\,\Delta\phi}{2\pi(0.015\,\text{s})} = 106.10\,\Delta\phi \tag{13.124}$$

So, a constant multiplier of 106.10 is applied to the output of the four-quadrant arctangent function.

*Noise Masking* Sometimes after the phase difference reconstruction, a noise mask is applied. With the standard magnitude images, regions of no signal (e.g., air) appear dark in the image because the intensity is confined to the lowest values of the dynamic range. In phase difference images, however, the noise background covers the entire dynamic range of image intensities. Consequently, the noise in air has a characteristic salt-and-pepper pattern. If this background is distracting or makes the window-level operation difficult, the noise from air can be suppressed by any of several masking techniques.

The common noise-masking methods employ a magnitude image reconstructed from the same raw data as is used to reconstruct the phase difference map. Suppose $M$ is the magnitude image corresponding to the phase difference map $\Delta\phi$. For example, in the multiple-coil case, $M$ could be calculated with (Bernstein et al. 1994).

$$M = \sqrt{\left|\sum_j \frac{Z_{1j} Z_{2j}^*}{\sigma_j^2}\right|} \tag{13.125}$$

Then the phase difference map can be masked using a threshold $M_0$:

$$\Delta\phi_{\text{thresh}} = \begin{cases} \Delta\phi & M \geq M_0 \\ 0 & M < M_0 \end{cases} \tag{13.126}$$

The threshold value $M_0$ can either be a predetermined constant or extracted from a histogram of the pixel values in $M$.

An alternative noise-masking method is to multiply the phase difference image by the magnitude image on a pixel-by-pixel basis:

$$\Delta\phi_{\text{mult}} = M\,\Delta\phi \tag{13.127}$$

The threshold and multiplicative masking methods each has its own advantages and pitfalls. The threshold method does not alter the phase difference pixel values (unless they are zeroed), which is convenient for extracting



quantitative information. The threshold method has the drawback that overaggressive masking can zero out pixel values that are of interest and setting a proper threshold value can require operator intervention. Conversely, the multiplicative masking method retains all the pixel values, but the mask must be divided out later if the true phase difference information is desired, for example, for quantitative flow analysis. Finally, we note that not using any masking method at all is a viable alternative because with practice it is not too difficult for the viewer to adapt to high dynamic range of the noise from air in unmasked phase difference maps.

### SELECTED REFERENCES


Bernstein, M. A., and Frigo, F. J. 1995. Gradient non-linearity correction for phase difference images. In *Proceedings of the 3rd Annual Meeting SMR*, p. 739.

Bernstein, M. A., Grgic, M., Brosnan, T. J., and Pelc, N. J. 1994. Reconstructions of phase contrast, phased array multicoil data. *Magn. Res. Med.* 32: 330–334.

Bernstein, M. A., Zhou, X. J., Polzin, J. A., King, K. F., Ganin, A., Pelc, N. J., and Glover, G. H. 1998. Concomitant gradient terms in phase contrast MR: Analysis and correction. *Magn. Res. Med.* 39: 300–308.

Ishihara, Y., Calderon, A., Watanabe, H., Okamoto, K., Suzuki, Y., Kuroda, K., and Suzuki, Y. 1995. A precise and fast temperature mapping using water proton chemical shift. *Magn. Reson. Med.* 34: 814–823.

Kernighan, B. W., and Ritchie, D. M. 1998. *The C programming language*. Upper Saddle Mountain: Prentice Hall.

Liang, Z. P. 1996. A model based phase unwrapping method. *IEEE Trans. Med. Imaging* 15: 893–897.

Moran, P. R., Moran, R. A., and Karstaedt, N. 1985. Verification and evaluation of internal flow and motion. True MRI by the phase gradient modulation method. *Radiology* 154: 433–441.

Muthupillai, R., Lomas, D. J., Rossman, P. J., Greenleaf, J. F., Manduca, A., and Ehman, R. L. 1995. Magnetic resonance elastography by direct visualization of propagating acoustic strain waves. *Science* 269: 1854–1857.

O'Donnell, M. 1985. NMR blood flow imaging using multiecho, phase contrast sequences. *Med. Phys.* 12: 59–64.


### RELATED SECTIONS

Section 10.1 Concomitant-Field Correction Gradient
Section 13.1 Fourier Reconstruction
Section 15.2 Phase-Contrast Angiography

## 13.6 View Sharing

*View sharing* (Riederer et al. 1988; Foo et al. 1995; Markl and Hennig 2001) is a reconstruction method that reuses some of the same k-space data